



Conditional normalizing flows for IceCube event reconstruction

Downloaded from: <https://research.chalmers.se>, 2025-06-02 22:08 UTC

Citation for the original published paper (version of record):

Abbasi, R., Ackermann, M., Adams, J. et al (2024). Conditional normalizing flows for IceCube event reconstruction. *Proceedings of Science*, 444

N.B. When citing this work, cite the original published paper.

Conditional normalizing flows for IceCube event reconstruction

The IceCube Collaboration

(a complete list of authors can be found at the end of the proceedings)

E-mail: thorsten.gluesenkamp@physics.uu.se

The IceCube Neutrino Observatory is a cubic-kilometer high-energy neutrino detector deployed in the Antarctic ice. Two major event classes are charged-current electron and muon neutrino interactions. In this contribution, we discuss the inference of direction and energy for these classes using conditional normalizing flows. They allow to derive a posterior distribution for each individual event based on the raw data that can include systematic uncertainties, which makes them very promising for next-generation reconstructions.

For each normalizing flow we use the differential entropy and the KL-divergence to its maximum entropy approximation to interpret the results. The normalizing flows correctly incorporate complex optical properties of the Antarctic ice and their relation to the embedded detector. For showers, the differential entropy increases in regions of high photon absorption and decreases in clear ice. For muons, the differential entropy strongly correlates with the contained track length. Coverage is maintained, even for low photon counts and highly asymmetrical contour shapes. For high-photon counts, the distributions get narrower and become more symmetrical, as expected from the asymptotic theorem of Bernstein-von-Mises. For shower directional reconstruction, we find the region between 1 TeV and 100 TeV to potentially benefit the most from normalizing flows because of azimuth-zenith asymmetries which have been neglected in previous analyses by assuming symmetrical contours. Events in this energy range play a vital role in the recent discovery of the galactic plane diffuse neutrino emission.

Corresponding authors: Thorsten Glüsenkamp^{1*}

¹ *Uppsala University, Uppsala, Sweden*

* Presenter

The 38th International Cosmic Ray Conference (ICRC2023)
26 July – 3 August, 2023
Nagoya, Japan



1. Introduction

High-energy neutrino astronomy emerged in the last decade, starting with the discovery of a diffuse neutrino flux in 2013 [1]. In 2017, the first evidence for a neutrino source, the blazar TXS 0506+056, was found using a FERMI-LAT gamma-ray follow-up of a neutrino alert and historical analysis of neutrino data [2]. In 2020, the point source search analysis improved by modeling the signal probability density function based on reconstructed quantities [3], which solved previous shortcomings in per-event contour coverage. It led to the first time-independent discovery of a neutrino source, the Seyfert galaxy NGC 1068. This new approach allowed for unbiased estimation of point source spectral parameters but sacrificed some sensitivity by averaging over events. Deep learning techniques, specifically conditional normalizing flows, now offer the potential to model non-symmetrical per-event uncertainties with correct coverage and improve point source capabilities yet again. Some initial studies regarding their performance for electron and muon neutrino charged current interactions are discussed in the following.

2. Conditional normalizing flows

Normalizing flows define flexible d -dimensional probability density functions and are defined with a change of basis formula via

$$p_{\theta}(x) = p_0(f_{\theta}^{-1}(x)) \cdot |\det J_{\theta}^{-1}(x)|, \quad (1)$$

where x is a d -dimensional vector, f_{θ} a bijective and differentiable function with parameters θ and J is the Jacobian of f . The base distribution p_0 is typically chosen to be a standard normal distribution in d dimensions, which has certain advantages for coverage calculations [4]. The parameters θ that define the flow-defining function f are the actual parameters of the PDF that is created in this way. One can introduce conditional dependency into the PDF by letting the flow parameters θ be the output of a neural network:

$$p_{\theta}(x|y) = p_0(f_{g_{\theta}(y)}^{-1}(x)) \cdot |\det J_{g_{\theta}(y)}^{-1}(x)| \quad (2)$$

The function g represents a neural network with parameters θ , which now are equivalent to the parameters that define the conditional PDF. Normalizing flows can be defined over Euclidean space, but also over manifolds like spheres [5]. For this contribution, we utilize three types of conditional normalizing flows. For the neutrino energy we use 1-d Euclidean flows consisting of two Gaussianization flow units [6] (f_G) and an affine flow (f_A). The target space is $\log_{10}(E_{\nu})$, i.e. the logarithm of the neutrino energy. For the neutrino direction we use 2-d spherical normalizing flows consisting of exponential-map flows with exponentiated potential [5] (f_E) and rotations (f_R). The exact definition of the flow-defining functions are given in table 1. All normalizing flows have been implemented in the open-source package `jammy_flows` [7] which has been used throughout this work. We use the coverage calculation for spherical flows as introduced in [4].

The neural network $g_{\theta}(x)$ (see eq. 2) is a graph neural network with base architecture as defined in [8], whose output is mapped via a multilayer-perceptron (MLP) to all the flow parameters. The difference with respect to the architecture in [8] is that the input features are not individual photon hit information, but a list of summary statistics of the noise-cleaned photon hits in a given optical module. Furthermore we use different aggregation functions and non-linearities.

type	flow function
1-d Euclidean	$f(z) = [f_A \circ f_G \circ f_G](z)$
2-d spherical	$f(z) = [(f_R \circ f_E)^8](z)$

Table 1: Flow definitions used for individual 1-d Euclidean and 2-d spherical flows. Iterative nesting of the bijective flow functions is indicated by \circ .

3. Reconstructions of IceCube events

Overview of training and coverage: We performed three neural-network training runs. Two of them were trained on ≈ 1.2 million events of electron-neutrino charged-current interactions to reconstruct a posterior over the neutrino energy (1d) or direction (2d). The third was trained on ≈ 1.4 million events of muon neutrino charged-current interactions to reconstruct a posterior over direction. The energy spectrum during training had a spectral index of -1.8 to obtain an approximately flat distribution after the detector response. The following visualizations and evaluations are performed on independent test datasets with ≈ 100000 events each. Example posteriors for two events with ≈ 10 TeV are shown in fig. 1. The first is a shower event in the "dust layer" (fig. 1a), a region roughly 2.1 km below the surface with a high dust concentration and therefore high photon absorption. Because of low optical transparency, the posterior region is spread out. The second is a shower event in the "clear ice" region (fig. 1b) situated between 2.3-2.4 km below the surface with particularly low dust contamination. The respective energy posteriors of the same events are approximately Gaussian (fig. 1c), but the dust layer event has a significantly larger uncertainty. In both example posteriors for the direction, the true direction is indicated by a red dot and lies in the respective 68% interval.

We used the methodology to calculate coverage for normalizing flows introduced in [4] and apply it on the different topologies. Coverage indicates how often a true value falls within a certain expected probability contour, which is what we call "observed" coverage compared to the "expected" contour containment. Fig. 2 shows the coverage behavior for shower direction, shower energy, and muon direction - split up into different categories. The muon direction coverage is only shown for the up- and downgoing sets, as the depth of the interaction position is not meaningful for arbitrarily aligned tracks. Coverage is within a few percent, even for asymmetric contour shapes.

Quantifying non-symmetrical PDF shapes with information theory: In the following we calculate symmetric maximum entropy approximations to the normalizing-flow distributions. For the Euclidean normalizing flow, the maximum-entropy approximation is a Gaussian distribution. For the spherical normalizing flow, the symmetric maximum-entropy approximation corresponds to a Fisher-von-Mises (FvM) distribution. We then calculate two information-theoretic quantities to draw conclusions about each individual event: the differential entropy for a performance measure and the KL-divergence between the exact distribution and the approximation for a measure of asymmetrical contour shapes.

A useful quantity to gauge the reconstruction performance for non-symmetric distributions is

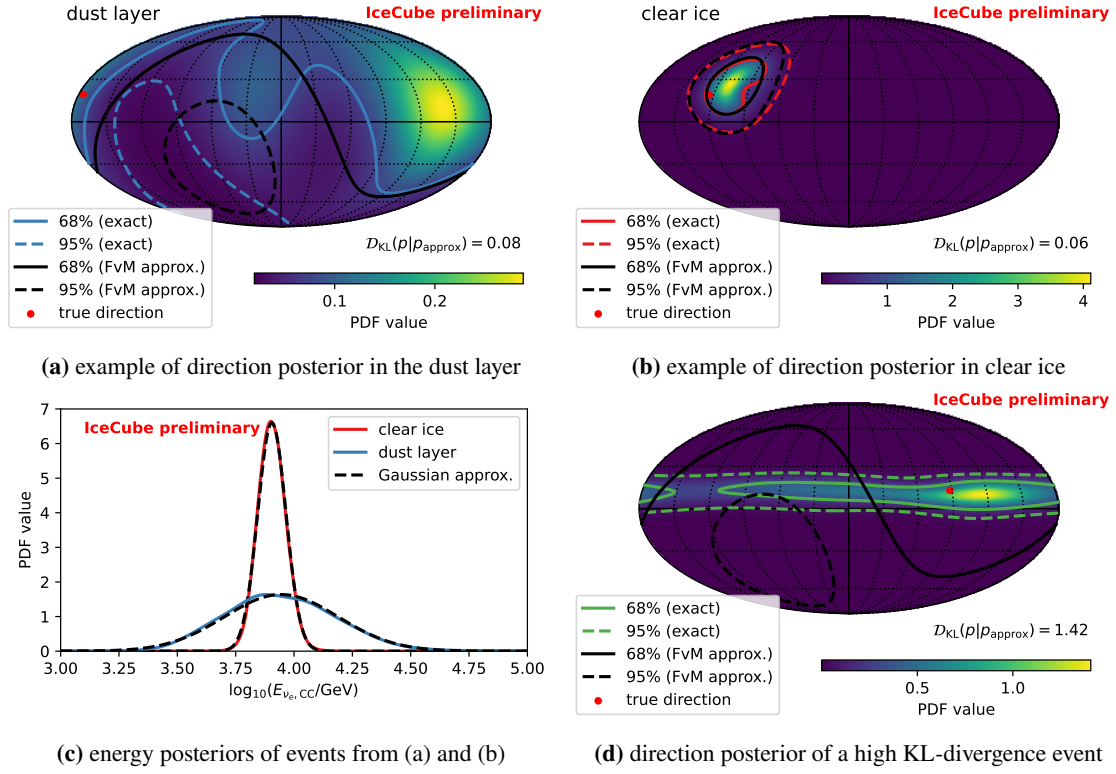


Figure 1: Visualizations of directional and energy posterior regions for two ν_e charged-current events with about 10 TeV neutrino energy. The event shown in a) is located in the dust layer, while the event shown in b) is located in a clearer ice region. The corresponding energy posteriors are shown in (c). The true values for the directions are indicated as red dots. Also shown is an example with high KL-divergence (d) as discussed in section 3. The respective Fisher-von-Mises and Gaussian approximations are depicted in black or black-dashed.

the differential entropy S_d . It is defined as

$$S_d[p(x)] = - \int p(x) \ln(p(x)) dx, \quad (3)$$

and measures how spread out the distribution is. To first order, it is useful to think about it as being proportional to the logarithm of the variance, as we have the closed-form solutions

$$S_d[\mathcal{G}_{1d}] = \frac{1}{2} + \frac{1}{2} \ln(2\pi\sigma_{68}^2) \quad (4)$$

$$S_d[\mathcal{G}_{2d}] = 1 + \ln(2\pi\sigma_{39}^2) \quad (5)$$

for a 1-d Gaussian and symmetric 2-d Gaussian, respectively. The latter is the differential entropy for the approximation of the Fisher-von-Mises distribution for large κ

$$\text{FvM}(x; \mu, \kappa) = \frac{\kappa \cdot \exp(\kappa \cdot \vec{\mu}^T \vec{x})}{2\pi \cdot (e^\kappa - e^{-\kappa})} \xrightarrow{\kappa \rightarrow \infty} \frac{\kappa \cdot \exp(\kappa \cdot \cos(\alpha))}{2\pi \cdot e^\kappa} \quad (6)$$

$$\xrightarrow{\alpha \rightarrow 0} \frac{\kappa}{2\pi} \cdot \exp\left(-\frac{1}{2}\kappa\alpha^2\right) = \frac{1}{2\pi\sigma_{39}^2} \cdot \exp\left(-\frac{1}{2}\frac{\alpha^2}{\sigma_{39}^2}\right), \quad (7)$$

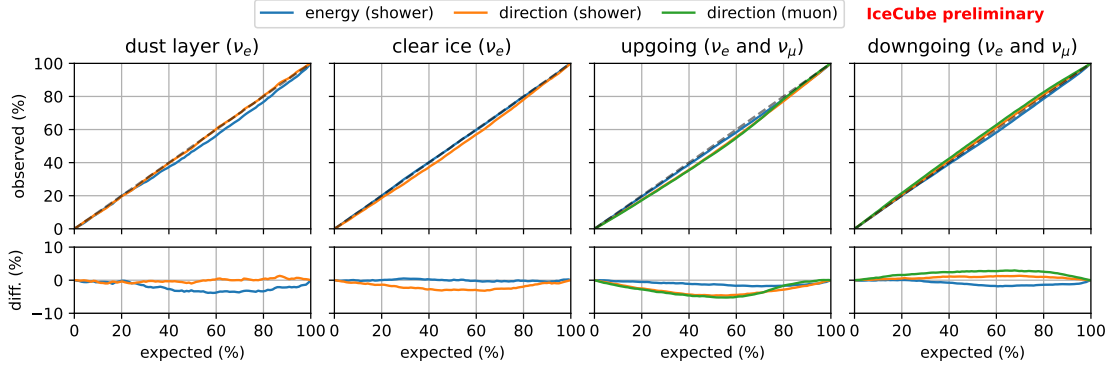


Figure 2: Coverage (explained in the text) for electron neutrino direction, electron neutrino energy, and muon direction PDFs for four different types of events. The events in the dust layer and clear ice region are selected based on the depth of the neutrino interaction, and are only shown for electron neutrinos.

where α is the angle between $\vec{\mu}$ and \vec{x} and σ_{39} is the standard deviation of the 2-d Gaussian approximation for small angles. In the end one obtains a simple relation between the κ parameter of the Fisher-von-Mises distribution and σ_{39} . The Gaussian is a reasonable approximation for $\kappa \gtrsim 30$ which corresponds to $\sigma_{39} \lesssim 10^\circ$. We make use of these relations later to plot the equivalent σ_{68} (1-d) and σ_{39} (2-d) values for a given entropy, for both energy and direction, respectively. In order to gauge how non-Gaussian (or for the sphere how non-symmetrical) a particular distribution is, we calculate the KL-divergence between the distribution and its respective maximum entropy approximation with similar first and second order moments. The forward KL-divergence is defined as

$$\mathcal{D}_{\text{KL}}(p(x)|p_{\text{approx.}}(x)) = \int p(x) \log \left(\frac{p(x)}{p_{\text{approx.}}(x)} \right) dx, \quad (8)$$

which is a distance measure between distributions. For the energy distribution, the maximum entropy approximation is a Gaussian distribution. For the directional distribution, we use a FvM distribution, which is a standard assumption in Icecube analyses. Those maximum-entropy approximations are fitted to 10000 samples drawn from the respective normalizing flow. If the normalizing flow is very asymmetric, it will have a large "distance" to its corresponding maximum entropy approximation. Since normalizing flows allow to produce samples, we can calculate both the entropy and the KL divergence as sampled-based expectation values for each event.

Energy reconstruction of $\nu_{e,CC}$ events: Results for the energy reconstruction are shown in fig. 3, which depicts the mean of the distribution versus the true energy (left), and versus the depth of interaction (right). The difference between the mean of the normalizing-flow distribution and the true value is centered around zero, with some exception towards the borders of the training dataset range. The spread is smallest in the region around one hundred TeV, and large inside the dust layer, and both of them are reflected in the differential entropy being small and large, respectively. This self-consistency has to happen, in order for coverage (fig 2) to hold. The KL divergence shows that towards smaller energies, in particular, the distributions become less Gaussian. Towards larger energies above $\approx 1\text{PeV}$ the decrease in resolution is likely due to low training statistics, although it could also in principle be due to PMT saturation effects becoming stronger. This will be looked at

in some future study.

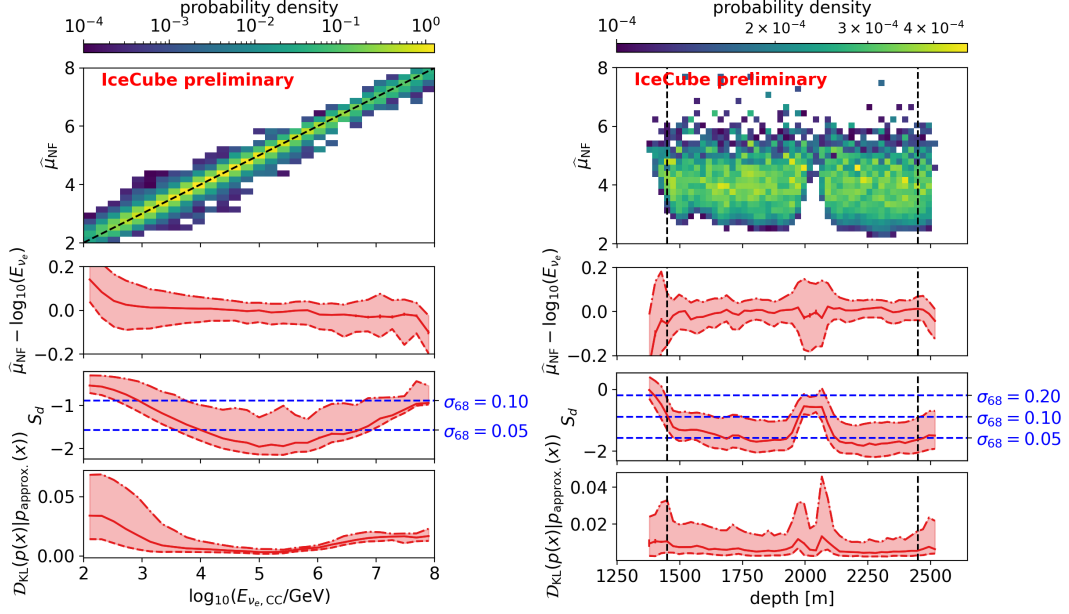


Figure 3: Sample mean $\hat{\mu}_{\text{NF}}$ of the normalizing-flow distribution over $\log_{10}(E_{\nu, \text{CC}})$ versus $\log_{10}(E_{\nu, \text{CC}})$ (left) and depth below the surface (right). The second, third, and fourth row show 16 (dashed), 50 (solid) and 84 (dash-dotted) percentiles of the difference of the true value from the mean, the differential entropy, and the KL-divergence, respectively. Indicated in blue are σ_{68} values of the corresponding Gaussian with equivalent entropy to gauge the entropy values. All events are weighted with an $E^{-1.8}$ energy spectrum. The detector boundary is indicated by the dashed black vertical lines.

Directional reconstruction of $\nu_{e, \text{CC}}$ events: Results for the directional reconstruction are shown in fig. 4 which depicts the logarithm of the angular resolution calculated with the mean μ of the distributions. The left figure shows the angular resolution as a function of energy. It shows that the posterior size reaches the equivalent of a 5 – 10 degree 2-d Gaussian around 100 TeV, which is close to existing shower reconstructions [9]. The KL-divergence indicates a class of events between 1 to 100 TeV that are more asymmetrical. Visual inspection (see fig. 1d) shows that these are events with large azimuthal uncertainty. Symmetric reconstructions based on a FvM distribution would fail to describe such events and overpredict the uncertainty. The recent analysis of the galactic plane [10] used the FvM assumption, and therefore could potentially be improved with normalizing flows. The right figure depicts the resolution as a function depth below the surface. The correlation to optical ice properties is clearly visible, and demonstrates that complex behavior is automatically learned by the normalizing flow.

Directional reconstruction of $\nu_{\mu, \text{CC}}$ events: Figure 5 depicts results for the spherical normalizing flow for muons. The logarithm of the angular resolution calculated with the mean μ of the distributions versus the cosine of the incident neutrino zenith is shown on the left. The performance is highest at the equator, with resolutions below one degree, and worse for up and downgoing directions. On the right of the figure, which shows the resolution as a function of contained track length, one can see a correlation of the performance with larger track lengths, as expected. While this performance likely does not match existing muon reconstructions yet, other encoding strategies that

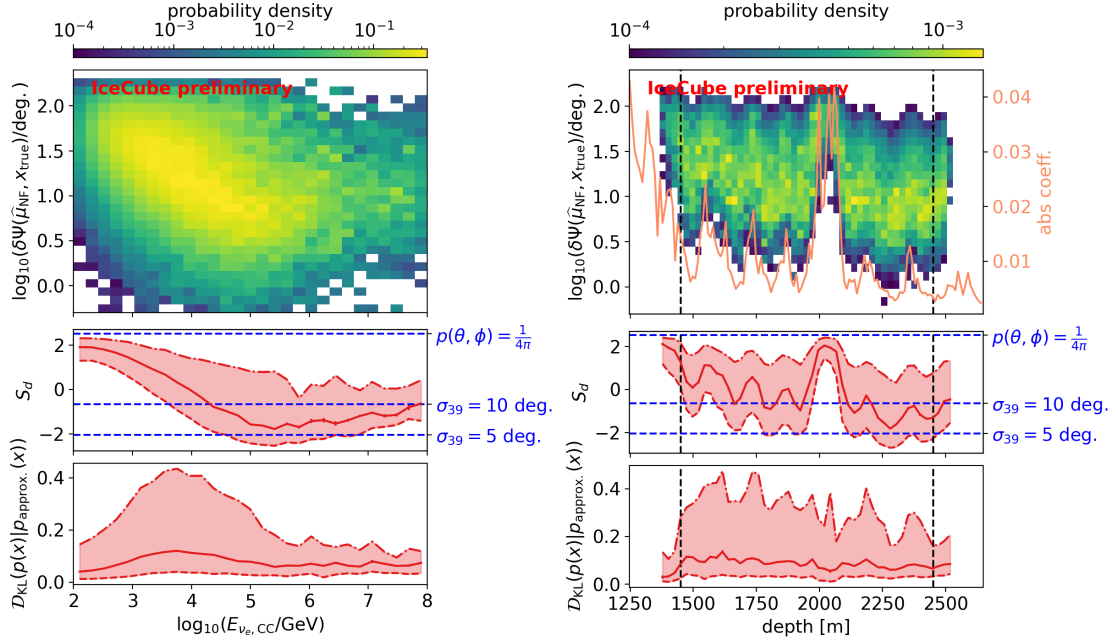


Figure 4: Logarithm of the angular distance between sample mean $\hat{\mu}_{\text{NF}}$ of the normalizing-flow distribution over the direction versus energy (left) and depth below the surface (right). The second and third row show 16 (dashed), 50 (solid) and 84 (dash-dotted) percentiles of the differential entropy, and the KL-divergence, respectively. Indicated in blue are values of σ_{39} of a 2-d Gaussian with equivalent entropy and the maximum entropy which corresponds to a flat distribution. All events are weighted with an $E^{-1.8}$ energy spectrum. The detector boundary is indicated by the dashed black vertical lines.

incorporate more label information for muons can achieve the performance of leading likelihood approaches, as was shown in [11]. The KL-divergence, which measures the asymmetry of contours, tends to be larger for more horizontal muon tracks and for tracks that are only partially contained. The asymmetry, however, is overall smaller than for electron neutrino showers.

4. Conclusion

In this contribution we trained conditional normalizing flows to learn the per-event posterior distributions over (log-)energy and direction of charged-current electron- and muon neutrinos in IceCube. The learned posterior distributions $p(\theta; x)$ directly use a summary statistic of the high-dimensional noise-cleaned photon data x as input. Coverage of these posteriors can be verified without numerical scans and is within a few percent of the expected values. For horizontal muon tracks, the median angular resolution of the normalizing-flow mean reaches below 1 degree. For electron neutrino showers, the angular normalizing flow approaches a performance of 5-10 degrees median angular resolution of the normalizing-flow mean around 100 TeV, which is comparable to state of the art likelihood approaches. We additionally find that between 1 and 100 TeV many electron neutrino events have large asymmetric uncertainties where the azimuth is much less constrained. For track reconstructions, the asymmetries tend to be smaller, but still detectable. In both cases, these asymmetric contours show the potential to improve on existing analyses, which currently utilize symmetric contour assumptions.

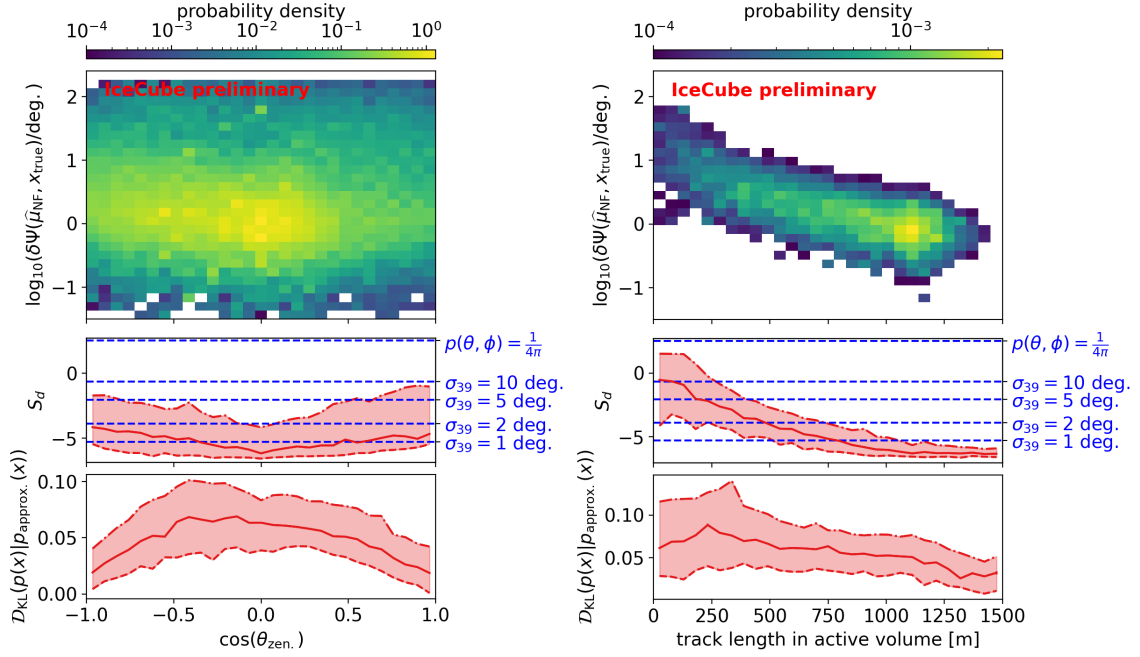


Figure 5: Logarithm of the angular distance between sample mean $\hat{\mu}_{\text{NF}}$ of the normalizing-flow distribution over the muon direction versus the cosine of the zenith direction (left) and muon length within the active detector volume (right). The second and third row show 16 (dashed), 50 (solid) and 84 (dash-dotted) percentiles of the differential entropy, and the KL-divergence, respectively. Indicated in blue are values of σ_{39} of a 2-d Gaussian with equivalent entropy and the maximum entropy which corresponds to a flat distribution. All events are weighted with an $E^{-1.8}$ energy spectrum.

Further interesting applications that are encouraged by these results are to use them for very low-energy events in oscillation analyses whose contours are expected to be non-Gaussian or real-time alert PDFs which require coverage guarantees.

References

- [1] The IceCube Collaboration *Physical Review Letters* **104** no. 2, (July, 2021) 022002.
- [2] The IceCube Collaboration *Science* **361** no. 6398, (2018) 147–151.
- [3] The IceCube Collaboration *Science* **378** no. 6619, (Nov., 2022) 538–543.
- [4] T. Glüsenskamp *arXiv e-prints* (Aug., 2020) arXiv:2008.05825.
- [5] D. J. Rezende *et al.*, “Normalizing flows on tori and spheres,” in *ICML*, pp. 8083–8092. 2020.
- [6] C. Meng, Y. Song, J. Song, and S. Ermon *arXiv e-prints* (Mar., 2020) arXiv:2003.01941.
- [7] T. Glüsenskamp (2023) https://github.com/thoglu/jammy_flows.
- [8] The IceCube Collaboration *Journal of Instrumentation* **17** no. 11, (Nov, 2022) P11003.
- [9] The IceCube Collaboration *PoS* **395** (Mar., 2022) 1065.
- [10] The IceCube Collaboration *Science* **380** no. 6652, (2023) 1338–1343.
- [11] The IceCube Collaboration *PoS* **395** (Mar., 2022) 1087.

Full Author List: IceCube Collaboration

R. Abbasi¹⁷, M. Ackermann⁶³, J. Adams¹⁸, S. K. Agarwalla^{40, 64}, J. A. Aguilar¹², M. Ahlers²², J.M. Alameddine²³, N. M. Amin⁴⁴, K. Andeen⁴², G. Anton²⁶, C. Argüelles¹⁴, Y. Ashida⁵³, S. Athanasiadou⁶³, S. N. Axani⁴⁴, X. Bai⁵⁰, A. Balagopal V.⁴⁰, M. Baricevic⁴⁰, S. W. Barwick³⁰, V. Basu⁴⁰, R. Bay⁸, J. J. Beatty^{20, 21}, J. Becker Tjus^{11, 65}, J. Beise⁶¹, C. Bellenghi²⁷, C. Benning¹, S. BenZvi⁵², D. Berley¹⁹, E. Bernardini⁴⁸, D. Z. Besson³⁶, E. Blaufuss¹⁹, S. Blot⁶³, F. Bontempo³¹, J. Y. Book¹⁴, C. Boscolo Meneguolo⁴⁸, S. Böser⁴¹, O. Botner⁶¹, J. Böttcher⁷, E. Bourbeau²², J. Braun⁴⁰, B. Brinson⁶, J. Brostean-Kaiser⁶³, R. T. Burley², R. S. Busse⁴³, D. Butterfield⁴⁰, M. A. Campana⁴⁹, K. Carloni¹⁴, E. G. Carnie-Bronca², S. Chattopadhyay^{40, 64}, N. Chau¹², C. Chen⁶, Z. Chen⁵⁵, D. Chirkin⁴⁰, S. Choi⁵⁶, B. A. Clark¹⁹, L. Classen⁴³, A. Coleman⁶¹, G. H. Collin¹⁵, A. Connolly^{20, 21}, J. M. Conrad¹⁵, P. Coppin¹³, P. Correa¹³, D. F. Cowen^{59, 60}, P. Dave⁶, C. De Clercq¹³, J. J. DeLaunay⁵⁸, D. Delgado¹⁴, S. Deng¹, K. Deoskar⁵⁴, A. Desai⁴⁰, P. Desati⁴⁰, K. D. de Vries¹³, G. de Wasseige³⁷, T. DeYoung²⁴, A. Diaz¹⁵, J. C. Díaz-Vélez⁴⁰, M. Dittmer⁴³, A. Domi²⁶, H. Dujmovic⁴⁰, M. A. DuVernois⁴⁰, T. Ehrhardt⁴¹, P. Eller²⁷, E. Ellinger⁶², S. El Mentawi¹, D. Elsässer²³, R. Engel^{31, 32}, H. Erpenbeck⁴⁰, J. Evans¹⁹, P. A. Evenson⁴⁴, K. L. Fan¹⁹, K. Fang⁴⁰, K. Farrag¹⁶, A. R. Fazzari⁷, A. Fedynitch⁵⁷, N. Feigl¹⁰, S. Fiedlschuster²⁶, C. Finley⁵⁴, L. Fischer⁶⁷, D. Fox⁵⁹, A. Frankowiak¹¹, A. Fritz⁴¹, P. Fürst¹, J. Gallagher³⁹, E. Ganster¹, A. Garcia¹⁴, L. Gerhardt⁹, A. Ghadimi⁵⁸, C. Glaser⁶¹, T. Glauch²⁷, T. Glusenkamp^{26, 61}, N. Goehke³², J. G. Gonzalez⁴⁴, S. Goswami⁵⁸, D. Grant²⁴, S. J. Gray¹⁹, O. Gries¹, S. Griffin⁴⁰, S. Griswold⁵², K. M. Groth²², C. Günther¹, P. Gutjahr²³, C. Haack²⁶, A. Hallgren⁶¹, R. Halliday²⁴, L. Halve¹, F. Halzen⁴⁰, H. Hamdaoui⁵⁵, M. Ha Minh²⁷, K. Hanson⁴⁰, J. Hardin¹⁵, A. A. Harnisch²⁴, P. Hatch³³, A. Haungs³¹, K. Helbing⁶², J. Hellrung¹¹, F. Henningsen²⁷, L. Heuermann¹, N. Heyer⁶¹, S. Hickford⁶², A. Hidvegi⁵⁴, C. Hill¹⁶, G. C. Hill², K. D. Hoffman¹⁹, S. Hori⁴⁰, K. Hoshina^{40, 66}, W. Hou³¹, T. Huber³¹, K. Hultqvist⁵⁴, M. Hünnefeld²³, R. Hussain⁴⁰, K. Hymon²³, S. In⁵⁶, A. Ishihara¹⁶, M. Jacquart¹⁶, O. Janik¹, M. Jansson⁵⁴, G. S. Japaridze⁵, M. Jeong⁵⁶, M. Jin¹⁴, B. J. P. Jones⁴, D. Kang³¹, W. Kang⁵⁶, X. Kang⁴⁹, A. Kappes⁴³, D. Kappesser⁴¹, L. Kardum²³, T. Karg⁶³, M. Karle²⁷, A. Karle⁴⁰, U. Katz²⁶, M. Kauer⁴⁰, J. L. Kelley⁴⁰, A. Khatee Zathul⁴⁰, A. Kheirandish^{34, 35}, J. Kiryluk⁵⁵, S. R. Klein^{8, 9}, A. Kochocki²⁴, R. Koirala⁴⁴, H. Kolanoski¹⁰, T. Kontrimas²⁷, L. Köpke⁴¹, C. Kopper²⁶, D. J. Koskinen²², P. Koundal³¹, M. Kovacevich⁴⁹, M. Kowalski^{10, 63}, T. Kozynets²², J. Krishnamoorthi^{40, 64}, K. Kruijswijk³⁷, E. Krupczak²⁴, A. Kumar⁶³, E. Kun¹¹, N. Kurahashi⁴⁹, N. Lad⁶³, C. Lagunas Gualda⁶³, M. Lamoureux³⁷, M. J. Larson¹⁹, S. Latseva¹, F. Lauber⁶², J. P. Lazar^{14, 40}, J. W. Lee⁵⁶, K. Leonard DeHolton⁶⁰, A. Leszczyńska⁴⁴, M. Lincetto¹¹, Q. R. Liu⁴⁰, M. Liubarska²⁵, E. Lohfink⁴¹, C. Love⁴⁹, C. J. Lozano Mariscal⁴³, L. Lu⁴⁰, F. Lucarelli²⁸, W. Luszczyk^{20, 21}, Y. Lyu^{8, 9}, J. Madsen⁴⁰, K. B. M. Mahn²⁴, Y. Makino⁴⁰, E. Manao²⁷, S. Mancina^{40, 48}, W. Marie Sainte⁴⁰, I. C. Mariş¹², S. Marka⁴⁶, Z. Marka⁴⁶, M. Marsee⁵⁸, I. Martinez-Soler¹⁴, R. Maruyama⁴⁵, F. Mayhew²⁴, T. McElroy²⁵, F. McNally³⁸, J. V. Mead²², K. Meagher⁴⁰, S. Mechbal⁶³, A. Medina²¹, M. Meier¹⁶, Y. Merckx¹³, L. Merten¹¹, J. Micallef²⁴, J. Mitchell⁷, T. Montaruli²⁸, R. W. Moore²⁵, Y. Morii¹⁶, R. Morse⁴⁰, M. Moulai⁴⁰, T. Mukherjee³¹, R. Naab⁶³, R. Nagai¹⁶, M. Nakos⁴⁰, U. Naumann⁶², J. Necker⁶³, A. Negi⁴, M. Neumann⁴³, H. Niederhausen²⁴, M. U. Nisa²⁴, A. Noell¹, A. Novikov⁴⁴, S. C. Nowicki²⁴, A. Obertacke Pollmann¹⁶, V. O'Dell⁴⁰, M. Oehler³¹, B. Oeyen²⁹, A. Olivas¹⁹, R. Ørsøe²⁷, J. Osborn⁴⁰, E. O'Sullivan⁶¹, H. Pandya⁴⁴, N. Park³³, G. K. Parker⁴, E. N. Paudel⁴⁴, L. Paul^{42, 50}, C. Pérez de los Heros⁶¹, J. Peterson⁴⁰, S. Philippen¹, A. Pizzuto⁴⁰, M. Plum⁵⁰, A. Pontén⁶¹, Y. Popovych⁴¹, M. Prado Rodriguez⁴⁰, B. Pries²⁴, R. Procter-Murphy¹⁹, G. T. Przybylski⁹, C. Raab³⁷, J. Rack-Helleis⁴¹, K. Rawlins³, Z. Rechac⁴⁰, A. Rehman⁴⁴, P. Reichherzer¹¹, G. Renzi¹², E. Resconi²⁷, S. Reusch⁶³, W. Rhode²³, B. Riedel⁴⁰, A. Rifaie¹, E. J. Roberts², S. Robertson^{8, 9}, S. Rodan⁵⁶, G. Roellinghoff⁵⁶, M. Rongen²⁶, C. Rott^{53, 56}, T. Ruhe²³, L. Ruohan²⁷, D. Ryckbosch²⁹, I. Safa^{14, 40}, J. Saffer³², D. Salazar-Gallegos²⁴, P. Sampathkumar³¹, S. E. Sanchez Herrera²⁴, A. Sandrock⁶², M. Santander⁵⁸, S. Sarkar²⁵, S. Sarkar⁴⁷, J. Savelberg¹, P. Savina⁴⁰, M. Schaufel¹, H. Schieler³¹, S. Schindler²⁶, L. Schlickmann¹, B. Schlüter⁴³, F. Schlüter¹², N. Schmeisser⁶², T. Schmidt¹⁹, J. Schneider²⁶, F. G. Schröder^{31, 44}, L. Schumacher²⁶, G. Schwefer¹, S. Sclafani¹⁹, D. Seckel⁴⁴, M. Seikh³⁶, S. Seunarine⁵¹, R. Shah⁴⁹, A. Sharma⁶¹, S. Shefali³², N. Shimizu¹⁶, M. Silva⁴⁰, B. Skrzypek¹⁴, B. Smithers⁴, R. Snihur⁴⁰, J. Soedingrekso²³, A. Sogaard²², D. Soldin³², P. Soldin¹, G. Sommani¹¹, C. Spannfellner²⁷, G. M. Spiczak⁵¹, C. Spiering⁶³, M. Stamatikos²¹, T. Stanev⁴⁴, T. Stetzelberger⁹, T. Stürwald⁶², T. Stuttard²², G. W. Sullivan¹⁹, I. Taboada⁶, S. Ter-Antonyan⁷, M. Thiesmeyer¹, W. G. Thompson¹⁴, J. Thwaites⁴⁰, S. Tilav⁴⁴, K. Tollefson²⁴, C. Tönnis⁵⁶, S. Toscano¹², D. Tosi⁴⁰, A. Trettin⁶³, C. F. Tung⁶, R. Turcotte³¹, J. P. Twagirayezu²⁴, B. Ty⁴⁰, M. A. Unland Elorrieta⁴³, A. K. Upadhyay^{40, 64}, K. Upshaw⁷, N. Valtonen-Mattila⁶¹, J. Vandenbroucke⁴⁰, N. van Eijndhoven¹³, D. Vannerom¹⁵, J. van Santen⁶³, J. Vara⁴³, J. Veitch-Michaelis⁴⁰, M. Venugopal³¹, M. Vereecken³⁷, S. Verpoest⁴⁴, D. Veske⁴⁶, A. Vijai¹⁹, C. Walck⁵⁴, C. Weaver²⁴, P. Weigel¹⁵, A. Weindl³¹, J. Weldert⁶⁰, C. Wendt⁴⁰, J. Werthebach²³, M. Weyrauch³¹, N. Whitehorn²⁴, C. H. Wiebusch¹, N. Willey²⁴, D. R. Williams⁵⁸, L. Witthaus²³, A. Wolf¹, M. Wolf²⁷, G. Wrede²⁶, X. W. Xu⁷, J. P. Yanez²⁵, E. Yildizci⁴⁰, S. Yoshida¹⁶, R. Young³⁶, F. Yu¹⁴, S. Yu²⁴, T. Yuan⁴⁰, Z. Zhang⁵⁵, P. Zhelnin¹⁴, M. Zimmerman⁴⁰

¹ III. Physikalisches Institut, RWTH Aachen University, D-52056 Aachen, Germany

² Department of Physics, University of Adelaide, Adelaide, 5005, Australia

³ Dept. of Physics and Astronomy, University of Alaska Anchorage, 3211 Providence Dr., Anchorage, AK 99508, USA

⁴ Dept. of Physics, University of Texas at Arlington, 502 Yates St., Science Hall Rm 108, Box 19059, Arlington, TX 76019, USA

⁵ CTSPS, Clark-Atlanta University, Atlanta, GA 30314, USA

⁶ School of Physics and Center for Relativistic Astrophysics, Georgia Institute of Technology, Atlanta, GA 30332, USA

⁷ Dept. of Physics, Southern University, Baton Rouge, LA 70813, USA

⁸ Dept. of Physics, University of California, Berkeley, CA 94720, USA

⁹ Lawrence Berkeley National Laboratory, Berkeley, CA 94720, USA

¹⁰ Institut für Physik, Humboldt-Universität zu Berlin, D-12489 Berlin, Germany

¹¹ Fakultät für Physik & Astronomie, Ruhr-Universität Bochum, D-44780 Bochum, Germany

¹² Université Libre de Bruxelles, Science Faculty CP230, B-1050 Brussels, Belgium

- ¹³ Vrije Universiteit Brussel (VUB), Dienst ELEM, B-1050 Brussels, Belgium
¹⁴ Department of Physics and Laboratory for Particle Physics and Cosmology, Harvard University, Cambridge, MA 02138, USA
¹⁵ Dept. of Physics, Massachusetts Institute of Technology, Cambridge, MA 02139, USA
¹⁶ Dept. of Physics and The International Center for Hadron Astrophysics, Chiba University, Chiba 263-8522, Japan
¹⁷ Department of Physics, Loyola University Chicago, Chicago, IL 60660, USA
¹⁸ Dept. of Physics and Astronomy, University of Canterbury, Private Bag 4800, Christchurch, New Zealand
¹⁹ Dept. of Physics, University of Maryland, College Park, MD 20742, USA
²⁰ Dept. of Astronomy, Ohio State University, Columbus, OH 43210, USA
²¹ Dept. of Physics and Center for Cosmology and Astro-Particle Physics, Ohio State University, Columbus, OH 43210, USA
²² Niels Bohr Institute, University of Copenhagen, DK-2100 Copenhagen, Denmark
²³ Dept. of Physics, TU Dortmund University, D-44221 Dortmund, Germany
²⁴ Dept. of Physics and Astronomy, Michigan State University, East Lansing, MI 48824, USA
²⁵ Dept. of Physics, University of Alberta, Edmonton, Alberta, Canada T6G 2E1
²⁶ Erlangen Centre for Astroparticle Physics, Friedrich-Alexander-Universität Erlangen-Nürnberg, D-91058 Erlangen, Germany
²⁷ Technical University of Munich, TUM School of Natural Sciences, Department of Physics, D-85748 Garching bei München, Germany
²⁸ Département de physique nucléaire et corpusculaire, Université de Genève, CH-1211 Genève, Switzerland
²⁹ Dept. of Physics and Astronomy, University of Gent, B-9000 Gent, Belgium
³⁰ Dept. of Physics and Astronomy, University of California, Irvine, CA 92697, USA
³¹ Karlsruhe Institute of Technology, Institute for Astroparticle Physics, D-76021 Karlsruhe, Germany
³² Karlsruhe Institute of Technology, Institute of Experimental Particle Physics, D-76021 Karlsruhe, Germany
³³ Dept. of Physics, Engineering Physics, and Astronomy, Queen's University, Kingston, ON K7L 3N6, Canada
³⁴ Department of Physics & Astronomy, University of Nevada, Las Vegas, NV, 89154, USA
³⁵ Nevada Center for Astrophysics, University of Nevada, Las Vegas, NV 89154, USA
³⁶ Dept. of Physics and Astronomy, University of Kansas, Lawrence, KS 66045, USA
³⁷ Centre for Cosmology, Particle Physics and Phenomenology - CP3, Université catholique de Louvain, Louvain-la-Neuve, Belgium
³⁸ Department of Physics, Mercer University, Macon, GA 31207-0001, USA
³⁹ Dept. of Astronomy, University of Wisconsin–Madison, Madison, WI 53706, USA
⁴⁰ Dept. of Physics and Wisconsin IceCube Particle Astrophysics Center, University of Wisconsin–Madison, Madison, WI 53706, USA
⁴¹ Institute of Physics, University of Mainz, Staudinger Weg 7, D-55099 Mainz, Germany
⁴² Department of Physics, Marquette University, Milwaukee, WI, 53201, USA
⁴³ Institut für Kernphysik, Westfälische Wilhelms-Universität Münster, D-48149 Münster, Germany
⁴⁴ Bartol Research Institute and Dept. of Physics and Astronomy, University of Delaware, Newark, DE 19716, USA
⁴⁵ Dept. of Physics, Yale University, New Haven, CT 06520, USA
⁴⁶ Columbia Astrophysics and Nevis Laboratories, Columbia University, New York, NY 10027, USA
⁴⁷ Dept. of Physics, University of Oxford, Parks Road, Oxford OX1 3PU, United Kingdom
⁴⁸ Dipartimento di Fisica e Astronomia Galileo Galilei, Università Degli Studi di Padova, 35122 Padova PD, Italy
⁴⁹ Dept. of Physics, Drexel University, 3141 Chestnut Street, Philadelphia, PA 19104, USA
⁵⁰ Physics Department, South Dakota School of Mines and Technology, Rapid City, SD 57701, USA
⁵¹ Dept. of Physics, University of Wisconsin, River Falls, WI 54022, USA
⁵² Dept. of Physics and Astronomy, University of Rochester, Rochester, NY 14627, USA
⁵³ Department of Physics and Astronomy, University of Utah, Salt Lake City, UT 84112, USA
⁵⁴ Oskar Klein Centre and Dept. of Physics, Stockholm University, SE-10691 Stockholm, Sweden
⁵⁵ Dept. of Physics and Astronomy, Stony Brook University, Stony Brook, NY 11794-3800, USA
⁵⁶ Dept. of Physics, Sungkyunkwan University, Suwon 16419, Korea
⁵⁷ Institute of Physics, Academia Sinica, Taipei, 11529, Taiwan
⁵⁸ Dept. of Physics and Astronomy, University of Alabama, Tuscaloosa, AL 35487, USA
⁵⁹ Dept. of Astronomy and Astrophysics, Pennsylvania State University, University Park, PA 16802, USA
⁶⁰ Dept. of Physics, Pennsylvania State University, University Park, PA 16802, USA
⁶¹ Dept. of Physics and Astronomy, Uppsala University, Box 516, S-75120 Uppsala, Sweden
⁶² Dept. of Physics, University of Wuppertal, D-42119 Wuppertal, Germany
⁶³ Deutsches Elektronen-Synchrotron DESY, Platanenallee 6, 15738 Zeuthen, Germany
⁶⁴ Institute of Physics, Sachivalaya Marg, Sainik School Post, Bhubaneswar 751005, India
⁶⁵ Department of Space, Earth and Environment, Chalmers University of Technology, 412 96 Gothenburg, Sweden
⁶⁶ Earthquake Research Institute, University of Tokyo, Bunkyo, Tokyo 113-0032, Japan

Acknowledgements

The authors gratefully acknowledge the support from the following agencies and institutions: USA – U.S. National Science Foundation-Office of Polar Programs, U.S. National Science Foundation-Physics Division, U.S. National Science Foundation-EPSCoR, Wisconsin Alumni Research Foundation, Center for High Throughput Computing (CHTC) at the University of Wisconsin–Madison, Open Science

Grid (OSG), Advanced Cyberinfrastructure Coordination Ecosystem: Services & Support (ACCESS), Frontera computing project at the Texas Advanced Computing Center, U.S. Department of Energy-National Energy Research Scientific Computing Center, Particle astrophysics research computing center at the University of Maryland, Institute for Cyber-Enabled Research at Michigan State University, and Astroparticle physics computational facility at Marquette University; Belgium – Funds for Scientific Research (FRS-FNRS and FWO), FWO Odysseus and Big Science programmes, and Belgian Federal Science Policy Office (Belspo); Germany – Bundesministerium für Bildung und Forschung (BMBF), Deutsche Forschungsgemeinschaft (DFG), Helmholtz Alliance for Astroparticle Physics (HAP), Initiative and Networking Fund of the Helmholtz Association, Deutsches Elektronen Synchrotron (DESY), and High Performance Computing cluster of the RWTH Aachen; Sweden – Swedish Research Council, Swedish Polar Research Secretariat, Swedish National Infrastructure for Computing (SNIC), and Knut and Alice Wallenberg Foundation; European Union – EGI Advanced Computing for research; Australia – Australian Research Council; Canada – Natural Sciences and Engineering Research Council of Canada, Calcul Québec, Compute Ontario, Canada Foundation for Innovation, WestGrid, and Compute Canada; Denmark – Villum Fonden, Carlsberg Foundation, and European Commission; New Zealand – Marsden Fund; Japan – Japan Society for Promotion of Science (JSPS) and Institute for Global Prominent Research (IGPR) of Chiba University; Korea – National Research Foundation of Korea (NRF); Switzerland – Swiss National Science Foundation (SNSF); United Kingdom – Department of Physics, University of Oxford.